J. Fluid Mech. (1986), *vol.* 167, *pp.* 1–18
Printed in Great Britain

Nonlinear model predictions of bispectra of shoaling surface gravity waves

By STEVE ELGAR
College of Engineering, University of Idaho, Moscow, ID 83843, USA

AND R. T. GUZA
Scripps Institution of Oceanography, University of California, La Jolla, CA 92093, USA

(Received 19 July 1985)

Boussinesq-type nonlinear equations for waves propagating over a sloping bottom are shown to accurately model the evolving bispectra of a spectrum of non-breaking shoaling ocean-surface gravity waves. The model response to a variation of the gentle, constant beach slope and the amount of nonlinear (i.e. non-random) phase coupling in the initial conditions is also examined. Variation of these quantities results in relatively little change in the overall structural evolution of the bicoherence and biphase (related to the nonlinear modification of the wave shape). The apparent unimportance of bottom slope motivates consideration of constant-depth KdV equations. Simple analytic solutions are found for harmonic growth in the special case of a monochromatic primary wavetrain. The associated bispectral evolution is qualitatively similar to field observations and to predictions based on the full Boussinesq model for a sloping bottom.

1. Introduction

As ocean-surface gravity waves shoal the wave field can undergo substantial nonlinear evolution from its deep-water state. This nonlinear evolution can result in the development of secondary peaks at harmonics of the power-spectral peak frequency, and in phase speeds substantially different from those predicted by the linear dispersion relationship. Higher-order spectral quantities (i.e. bispectra) also evolve as the wave field shoals (Elgar & Guza 1985*b*). Bicoherence levels increase, indicating significant nonlinear coupling between Fourier modes. Biphases and sea-surface-elevation skewness and asymmetry (with respect to a vertical axis) evolve in a manner consistent with the change in wave shape from a nearly sinusoidal profile in deep (9 m depth) water to the pitched-forward profile observed just before wave breaking.

Linear finite-depth theory does not predict the transformation of many of the statistics of a shoaling wave field. A model based upon the nonlinear Boussinesq equations for a sloping bottom (Peregrine 1967) has been shown to be generally superior to linear finite-depth theory for the prediction of frequency-band energy and phase, and other low-order statistics of the wave field (Freilich & Guza 1984; Elgar & Guza 1985*a*). In the present study, the nonlinear model is shown to predict accurately the observed evolution of bispectral quantities.

Basic bispectral definitions and the bispectral evolution observed on a sloping beach are briefly summarized in §2. The nonlinear Boussinesq model equations are discussed in §3. Comparisons between model predictions and field data are made in

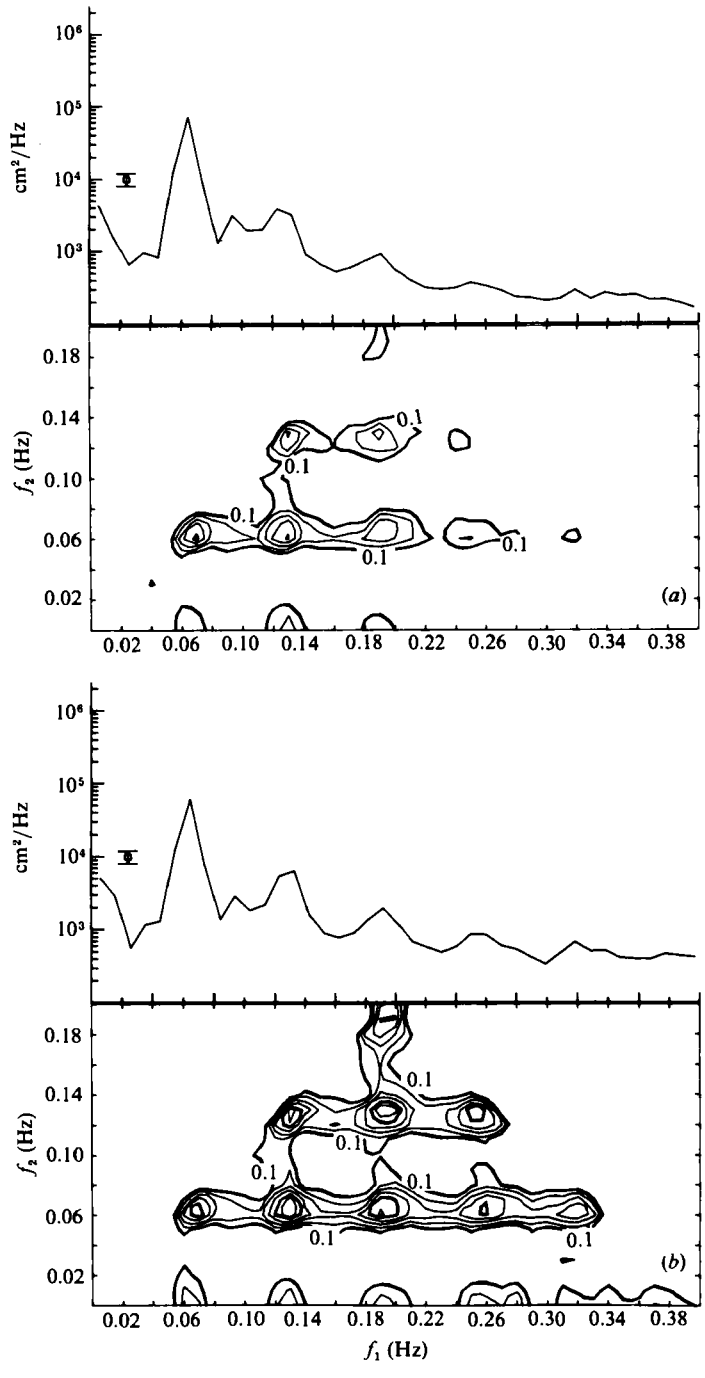

FIGURE 1. Power spectra and contours of bicoherence for the narrow-band 2 February data. The power spectra (bars indicate 95% confidence levels) are immediately above the corresponding bicoherence plots. Wave triads involve frequencies f_1, f_2, and f_1+f_2. The minimum value of bicoherence plotted is $b = 0.1$, with contours every 0.05. There are 250 degrees of freedom, and the 95% significance level for zero bicoherence is $b = 0.15$ (see Elgar & Guza 1985*b* for discussion of bicoherence significance levels). The significant wave height H_s (defined as 4 times the sea-surface standard deviation) is 65 cm in 4 m depth. (*a*) depth = 2.7 m; (*b*) 2.0 m.

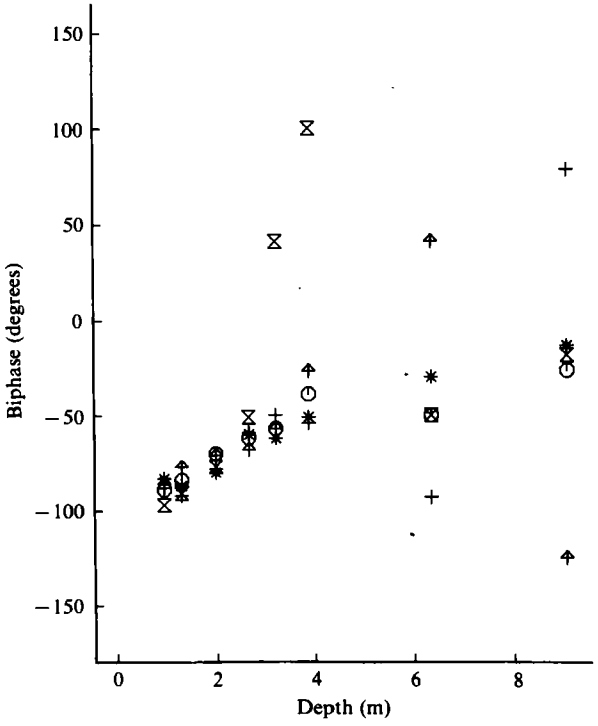

FIGURE 2. Biphase *versus* depth for selected frequency pairs for the 2 February data set. The symbols represent different wave triads; the two lower interacting frequencies are given, with the third frequency equal to their sum. ✱, (f,f); ⊙, $(f,2f)$; +, $(f,3f)$; ♠, $(2f,2f)$; ⧖, $(3f,3f)$, where $f = 0.06$ Hz corresponds to the power-spectral (figure 1) peak frequency.

§3.1, and the results of model simulations with zero beach slope and with different phase coupling in the initial conditions are presented in §§3.2 and 3.3 respectively. In view of the apparent unimportance of beach slope to overall bispectral evolution, equations for a constant-depth fluid are considered in §4. Analytic solutions for the particularly simple case of harmonic growth due to a single narrow-banded primary wavetrain are shown to qualitatively agree with the bispectral evolution observed in field data and predicted by the full Boussinesq model.

2. Definitions and field observations

The field observations were obtained in 1980, at Santa Barbara, California. The data considered here are from an array of near-bottom-mounted pressure sensors deployed along a cross-shore transect between 1 and 9 m depth, beach slope = 0.05. The sample rate was 2 Hz, and the data sets are several hours long. Descriptions of the sensors, instrument positioning, and data reduction are given in Elgar & Guza (1985*a*, *b*) and references therein.

For a discretely sampled process the (complex) bispectrum is defined as (Haubrich 1965; Kim & Powers 1979)

$$B(\omega_1, \omega_2) = \mathrm{E}[A_{\omega_1} A_{\omega_2} A^*_{\omega_1+\omega_2}], \tag{2.1}$$

where ω is the radian frequency, A is a complex Fourier coefficient and E[ ] is the expected value, or average, operator. The normalized magnitude and phase of the

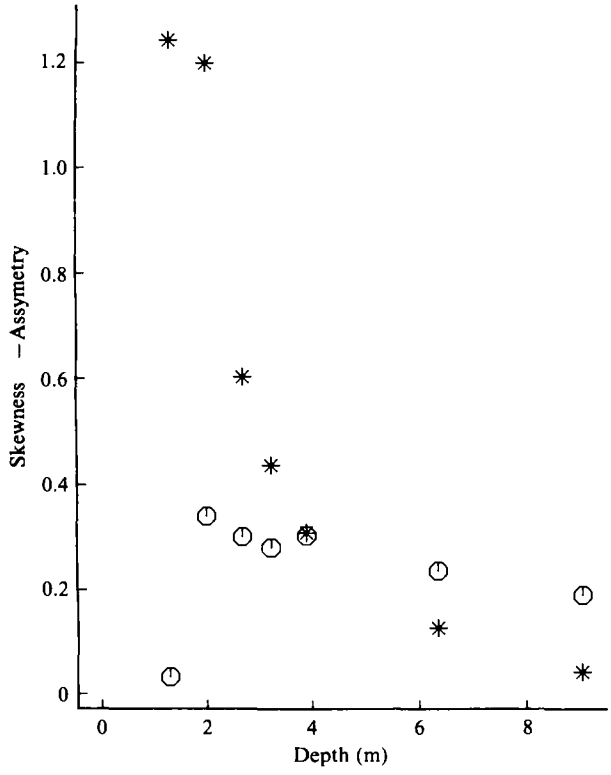

FIGURE 3. Skewness and −asymmetry *versus* depth for the 2 February data: ⊙, skewness; ✳, −asymmetry. The data have been band-pass filtered between 0.04 and 0.4 Hz.

bispectrum are the bicoherence and biphase, given respectively by (Kim & Powers 1979)

$$b^2(\omega_1, \omega_2) = \frac{|B(\omega_1, \omega_2)|^2}{\mathrm{E}[|A_{\omega_1} A_{\omega_2}|^2]\,\mathrm{E}[|A_{\omega_1+\omega_2}|^2]}, \tag{2.2}$$

$$\beta(\omega_1, \omega_2) = \arctan\left[\frac{\mathrm{Im}\{B(\omega_1, \omega_2)\}}{\mathrm{Re}\{B(\omega_1, \omega_2)\}}\right]. \tag{2.3}$$

For a narrow-band spectrum of waves, the bicoherence of wave triads involving the power-spectral peak frequency and its harmonics increases as the wave field shoals from 9 to 1 m depth (Elgar & Guza 1985*b*, hereinafter referred to as EG), indicating increasing phase coupling between these frequency bands. Bicoherences observed in 2.7 and 2.0 m depth are shown in figure 1. Figure 2 shows that the biphase between the power-spectral peak and its harmonics evolves from a value close to zero (consistent with Stokes-type nonlinear interactions, Hasselman, Munk & MacDonald 1963) in 9 m depth to about $\beta = -\frac{1}{2}\pi$ (the biphase of a sawtooth (EG)) in very shallow water (approximately 1 m in depth), an evolution distance of about 300 m. The biphase evolution is associated with the evolution of sea-surface-elevation skewness and asymmetry (with respect to a vertical axis), which are normalized sums of the real and imaginary parts of the bispectrum respectively (Hasselman *et al.* 1963; EG).

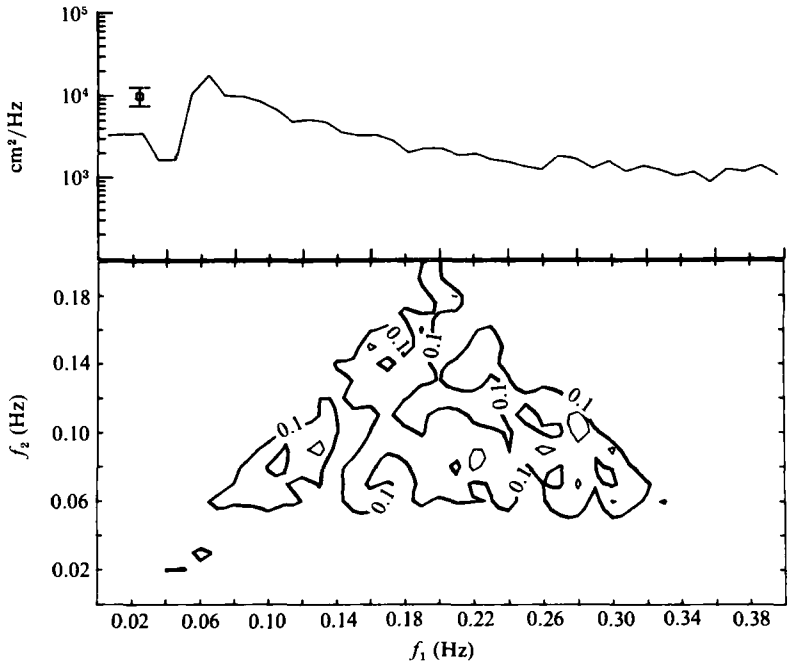

FIGURE 4. Power spectrum (above) and contours of bicoherence (below) for the broad-band 15 February data measured in 1.6 m depth. Format is the same as figure 1. There are 160 degrees of freedom, and the 95% significance level for zero bicoherence is $b = 0.19$. H_s in 4 m depth is 65 cm.

As shown in figure 3, the skewness is relatively low (but statistically different from zero) in 9 m depth, increases to a maximum in about 2 m depth, and then decreases to near zero in even shallower water where wave breaking is important. The asymmetry has a near-zero value in 9 m depth, and increases (in absolute value, asymmetry is negative for shoaling waves in the coordinate frame used here) nearly monotonically as the waves shoal.

Wave fields with broad-band power spectra in shallow water have moderate, but statistically significant, bicoherence levels over a wide range of frequency pairs (figure 4), indicating nonlinear coupling between many Fourier modes. The evolution of biphase, skewness and asymmetry in a broad-band wave field is remarkably similar to that observed in a narrow-band spectrum (EG and figure 8).

Bispectral calculations provide evidence for the excitation of Fourier modes by difference interactions as well as sum interactions in a wave field with a double-peaked power spectrum (figures 11 and 12 in EG). Unlike sum interactions (figure 2), biphases for triads involved in difference interactions evolve from $\beta = 180°$ in deep water to lower values as the wave field shoals (figure 12 in EG).

3. Boussinesq nonlinear model

Starting with the Boussinesq equations for waves travelling over a sloping bottom (Peregrine 1967), Freilich & Guza (1984) develop equations which describe the evolution of a wave field's Fourier components. Schematically, the differential

Set	Model depth	Amplitudes	Phases
S0		Field data	
S1	variable	4 m	measured
S2	variable	4 m	random
S3	2.5 m	9 m	measured
S4	2.5 m	9 m	random
S5	2.5 m	4 m	measured

TABLE 1. Model parameters. The amplitude column gives the depths at which the field data, used in the initial conditions, were collected. The phase column indicates whether if the measured initial power spectrum was coupled with measured Fourier phases or with random phases for the corresponding model set. The variable-depth cases had a beach slope = 0.05.

equations for Fourier amplitudes and phases are respectively

$$\left.\begin{aligned}
\dot{a}_n &= -a_n S_n + \sum_j a_j a_{n-j} R_{(j,\,n-j)} \sin(\Phi_j + \Phi_{n-j} - \Phi_n) \\
&\quad + \sum_j a_j a_{j-n} R_{(j,\,n-j)} \sin(\Phi_j - \Phi_{j-n} - \Phi_n) \\
&\quad + \sum_j a_j a_{n+j} R_{(n+j,\,-j)} \sin(\Phi_{n+j} - \Phi_j - \Phi_n), \\
\dot{\Phi}_n &= k_n - \sum_j \left(\frac{(a_j a_{n-j})}{a_n}\right) R_{(j,\,n-j)} \cos(\Phi_j + \Phi_{n-j} - \Phi_n) \\
&\quad - \sum_j \left(\frac{(a_j a_{j-n})}{a_n}\right) R_{(j,\,n-j)} \cos(\Phi_j - \Phi_{j-n} - \Phi_n) \\
&\quad - \sum_j \left(\frac{(a_j a_{n+j})}{a_n}\right) R_{(n+j,\,j)} \cos(\Phi_{n+j} - \Phi_j - \Phi_n),
\end{aligned}\right\} \tag{3.1}$$

where the overdot indicates differentiation with respect to the offshore coordinate x, and the coupling and shoaling coefficients (R_n and S_n) are functions of the radian frequency ω and the depth h [given in Freilich & Guza (1984), equations (21)–(24)]. The bottom slope appears explicitly only in the shoaling coefficient S_n. Equation (3.1) has linear wavenumber at mode n of $k_n = (\omega_n/(gh)^{\frac{1}{2}})\,(1 + h\omega_n^2/(6g))$. This dispersion equation is better behaved at high frequencies where formally equivalent (at this order) forms yield imaginary wavenumbers. The model [(3.1)] assumes that the waves are normally incident to a beach with plane-parallel contours, and that no energy is reflected or dissipated. Model predictions of the spatial evolution of spectra and cross-spectra are in good agreement with two different sets of observations (Freilich & Guza 1984; Elgar & Guza 1985*a*).

3.1. *Model-data comparisons*

The model-data comparisons are statistical. For each 512 s record of data, Fourier amplitudes and phases measured at the 4 m depth pressure sensor were used as initial conditions (this is model set number 1, hereafter denoted S1, in table 1; the field data are denoted S0) for the numerical integration of (3.1). The model spectra have 205 frequency bands evenly distributed between 0.00 and 0.4 Hz, and require integration of 410 first-order nonlinear differential equations for each 512 s initial condition. The numerical integrations yield predicted Fourier amplitudes and phases at shoreward locations. Many 512 s pieces were integrated, and the Fourier coefficients used to

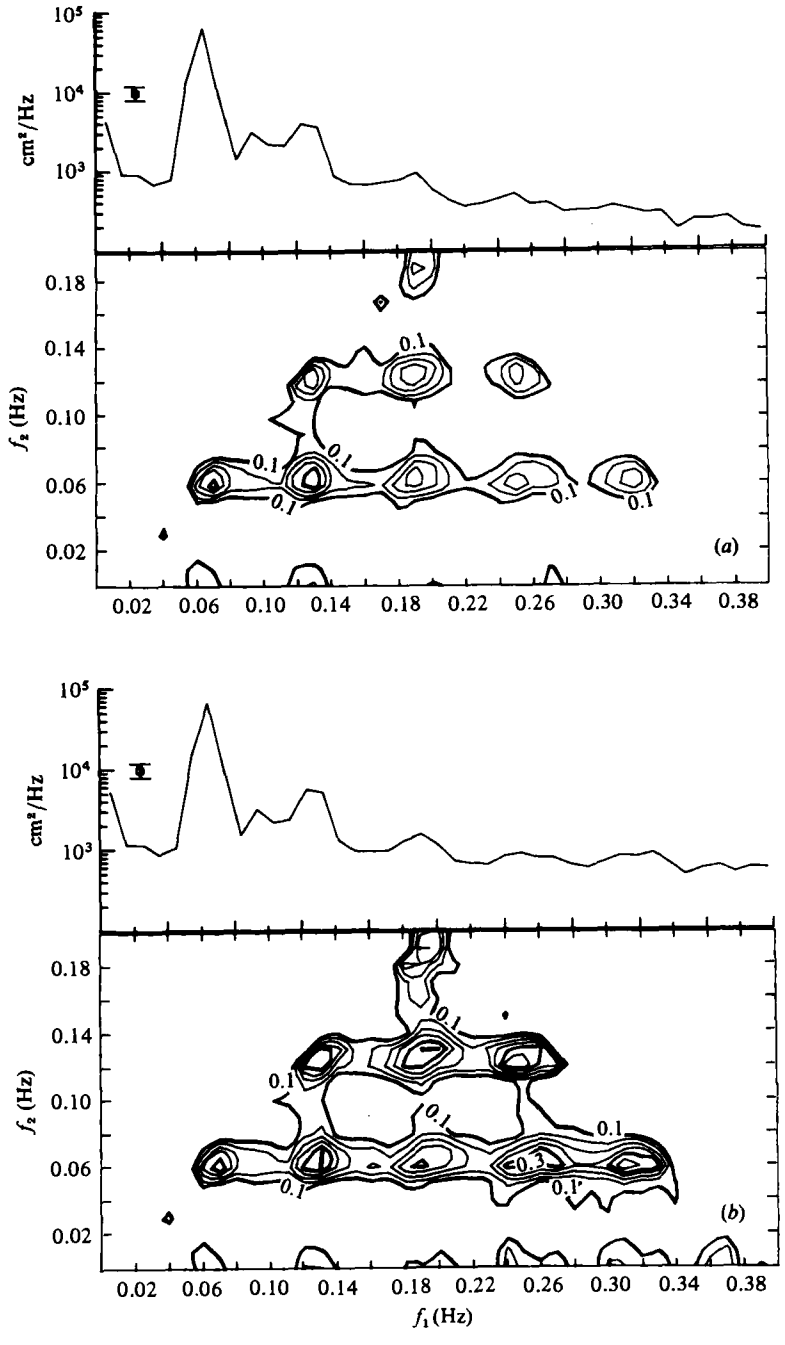

FIGURE 5. Power spectra and contours of bicoherence predicted by the spectral nonlinear model ((3.1)) for the 2 February data. See figure 1 for explanation of symbols. (*a*) 2.7 m depth; (*b*) 2.0 m.

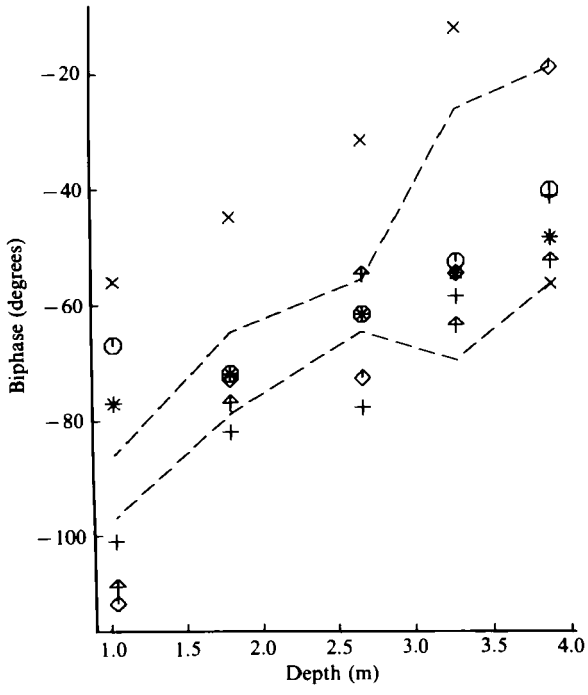

FIGURE 6. Biphase *versus* depth for selected frequency pairs for the 2 February spectral nonlinear-model ((3.1)) predictions. The dashed lines indicate the range of observed biphase values for the corresponding frequency pairs (figure 2). ✳, (f,f); ⊙, $(f,2f)$; +, $(f,3f)$; ×, $(f,4f)$; ⇑, $(2f,2f)$; ◇, $(2f,3f)$, where $f = 0.06$ Hz corresponds to the power-spectral peak frequency.

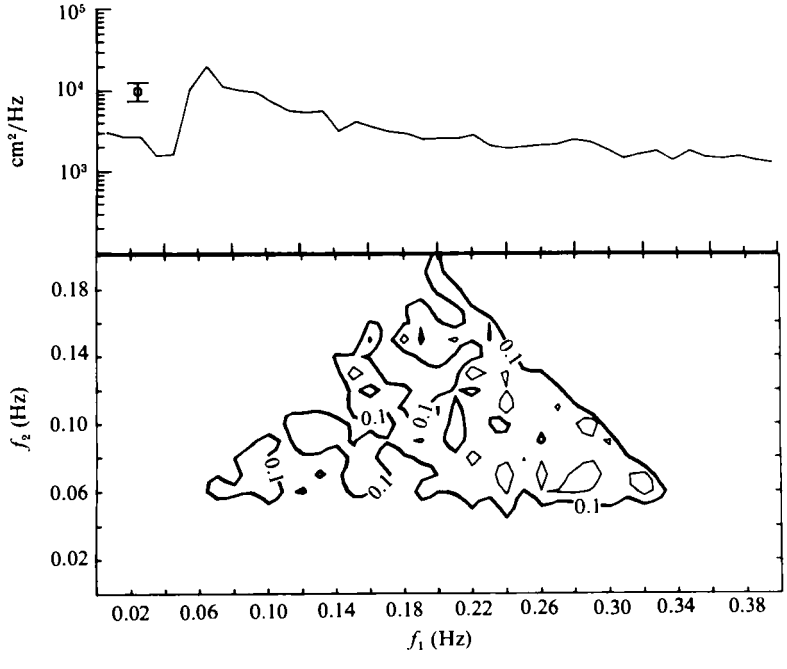

FIGURE 7. Power spectrum and contours of bicoherence predicted by the spectral nonlinear model ((3.1)) for the 15 February data for $h = 1.6$ m. See figure 4 for explanation of symbols.

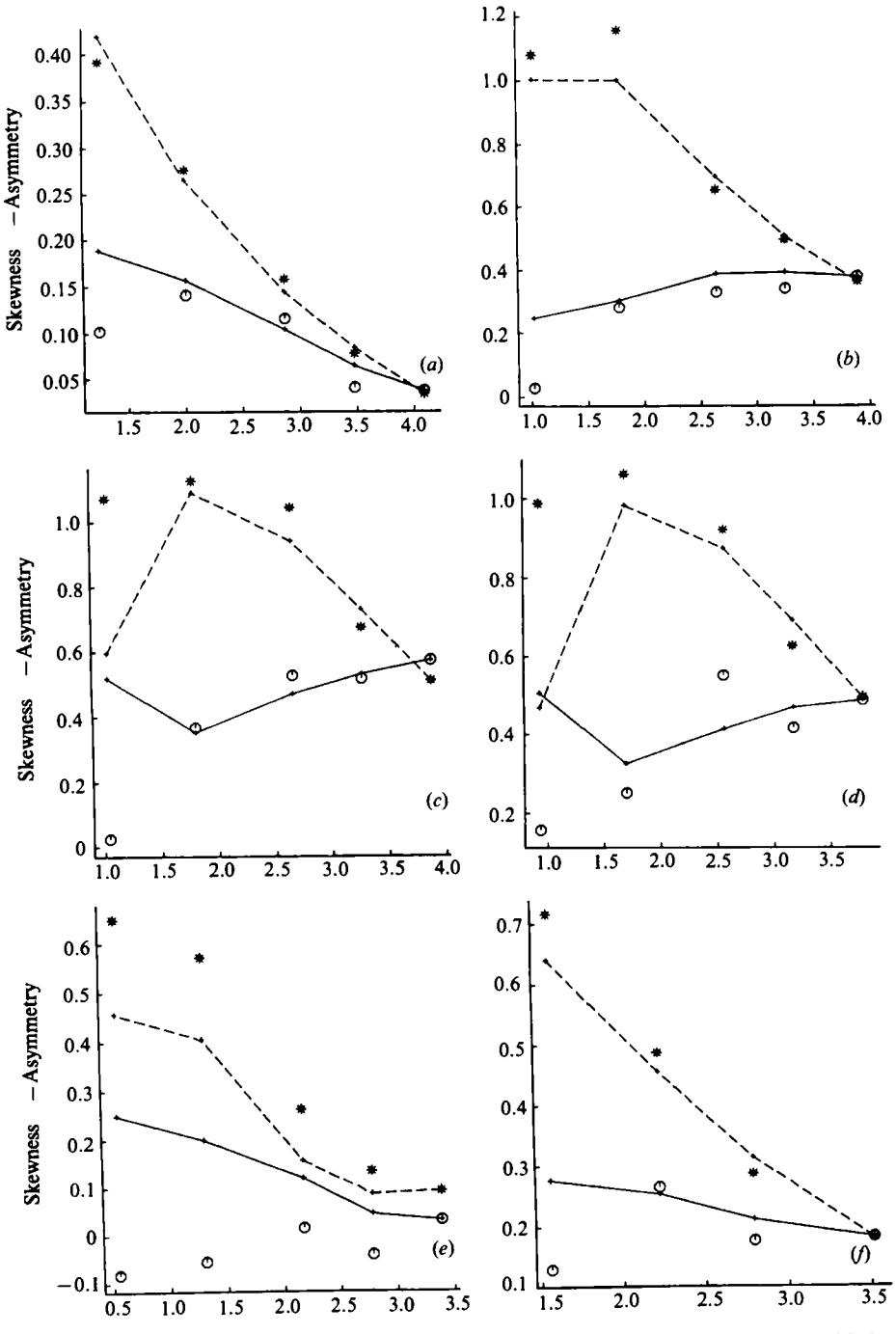

FIGURE 8. Sea-surface elevation skewness and −asymmetry *versus* depth from field data and as predicted by the nonlinear model. The records have been band-pass filtered between 0.04 and 0.3 Hz. *, −asymmetry of data; ⊙, skewness of data. Predicted values are: dashed line, −asymmetry; solid line, skewness. The data sets are described in detail in Elgar & Guza (1985*a*, table 1). Briefly, they are (*a*) 30 January, broad-band spectrum, $H_s = 33$ cm; (*b*) 2 February, narrow-band, $H_s = 65$ cm; (*c*) 3 February, narrow-band, $H_s = 93$ cm; (*d*) 4 February, narrow-band, $H_s = 88$ cm; (*e*) 12 February, double peaked, $H_s = 52$ cm; (*f*) 15 February, broad-band, $H_s = 65$ cm.

calculate bispectra (from (2.1)) with the same number of degrees of freedom as the bispectra of the observations.

The nonlinear-model predictions of bispectra agree quite well with the observations. For example, figure 5 displays the nonlinear-model predictions of bicoherence for the narrow-band data set, which are seen to be structurally similar to the observations (figure 1). Nonlinear-model predictions and observations of biphases for selected frequency pairs as a function of depth for the narrow-band data are shown in figure 6. The predicted biphase (not shown) and bicoherence (figure 7) for a broad-band data set also match the field data (figure 4) quite well. Model predictions of bicoherence and biphase for double-peaked power spectra (not shown) are similar to observations (EG, figures 11 and 12), including the sea–swell difference interactions discussed in EG.

Predicted and observed values of sea-surface-elevation skewness and asymmetry for several data sets (band-pass filtered between 0.04 and 0.3 Hz) are shown in figure 8. Except for the data with double-peaked power spectra (figure 8*e*), the nonlinear model accurately predicts the overall evolution of both skewness and asymmetry. The shallowest data points in figures 8(*c*, *d*), which are well inside the breaking region and may be strongly nonlinear, are not well predicted by the weakly nonlinear, non-dissipative model.

Comparisons between bispectral observations and model predictions for six data sets, including broad-band and narrow-band power spectra, with 4 m depth significant wave heights ranging from 33 to 92 cm were made. The comparisons shown here are a representative sample.

3.2. *Flat-bottom simulations*

Data obtained at a different location (Torrey Pines, California), where the beach slope = 0.02, have bispectral evolution quite similar to the data discussed above, where the beach slope = 0.05. In particular, biphase values for the Torrey Pines data approach $\beta = -\frac{1}{2}\pi$, and the absolute value of asymmetry monotonically increases from near zero in deep water to about 1 as the waves shoal. A vertical asymmetry similar to that observed in the field (figures 3 and 8), but much milder, has been theoretically predicted for cnoidal-wave solutions to nonlinear Boussinesq-type equations on a sloping bottom (Svendsen & Buhr-Hansen 1978). Shoaling monochromatic waves in the laboratory also become asymmetrical about a vertical axis, with biphases (all the frequencies were harmonics of the primary) approaching $\beta = -\frac{1}{2}\pi$ during shoaling and breaking (Flick, Guza & Inman 1981), similar to the field observations of EG. Svendsen & Buhr-Hansen (1978) and Flick *et al.* (1981) point out that in these cases the sloping bottom makes a critical contribution to the evolution of wave shape, since on a flat bottom cnoidal and Stokes waves have permanent form by definition. In the light of these observations of evolving wave shapes, it is of interest to compare model results with identical initial conditions, but with and without depth variations.

To investigate the effect of a gently sloping bottom on bispectral evolution, the nonlinear model ((3.1)) was numerically integrated for several cases of a shallow and constant (2.5 m) depth (S3–S5, table 1). Model set S3 uses 9 m depth measured Fourier amplitudes (figure 9) and phases as initial conditions. Model sets S4 and S5 (discussed again in §3.3) use initial conditions different from S3, see table 1.

As the wave field (for S3–S5) evolves over the 2.5 m depth flat bottom several features strikingly similar to the sloping-bottom cases (observed and simulated) appear. The bicoherence spectra for the 2.5 m depth flat-bottom simulations (S3 at

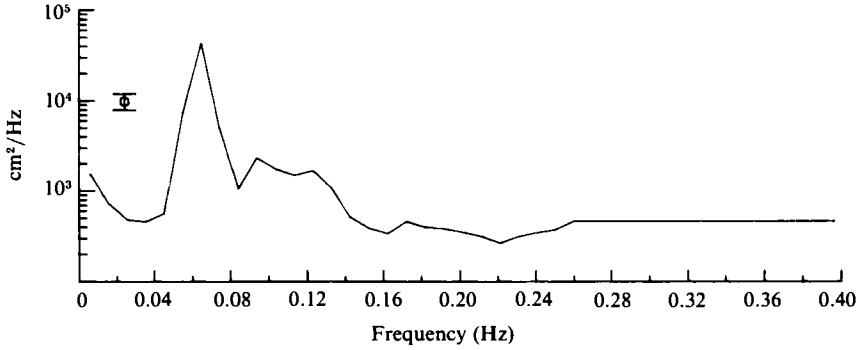

FIGURE 9. Power spectrum measured in 9 m depth, and used in the initial conditions for model sets S3 and S4. The bars indicate 95% confidence levels.

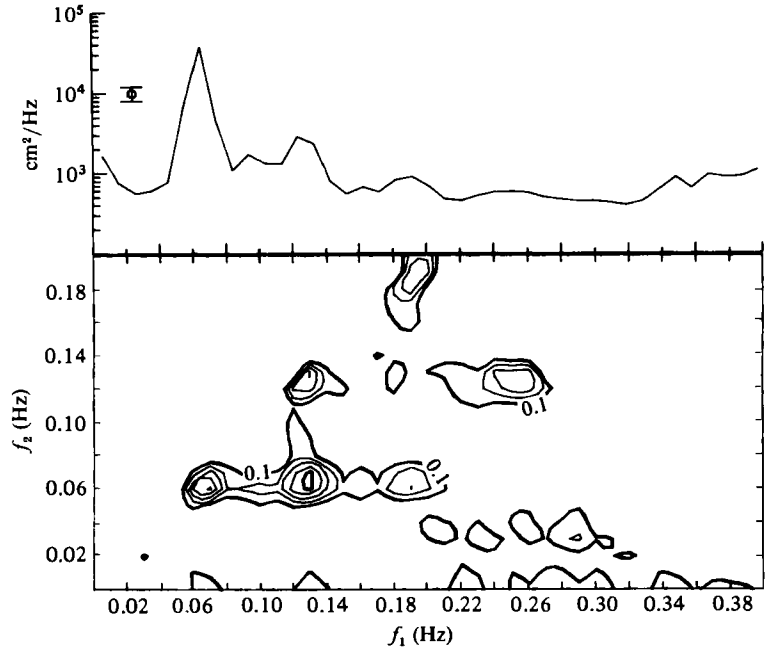

FIGURE 10. Power spectrum (above) and contours of bicoherence (below) predicted by the flat-bottom spectral nonlinear model at $x = 61$ m, with initial conditions S3. Format is the same as figure 1.

$x = 61$ m is shown in figure 10) resemble the field data (S0, figure 1*a*) in 2.7 m depth (S5 and S1 are also comparable). The chief discrepancy between S3 and S0 involves triads with a very high-frequency mode ($f > 0.3$ Hz), where the flat-bottom integrations tend to overpredict power-spectral levels (compare power spectra in figures 1*a* and 10). This overprediction of spectral levels at high frequencies by the nonlinear model (which is discussed in Elgar & Guza 1985*a*) led to unrealistic predicted power spectra at evolution distances greater than approximately 70 m. The 2.7 m depth field data are 255 m shoreward of those at 9 m depth. The difference in evolution distances (61 and 255 m) reflects the fact that nonlinear effects are stronger in shallow water. The point here is that the flat- and sloping-bottom solutions, with identical initial conditions, evolve to structurally similar states.

As illustrated in figure 11 for S3, all flat-bottomed test cases (S3–S5) show biphase

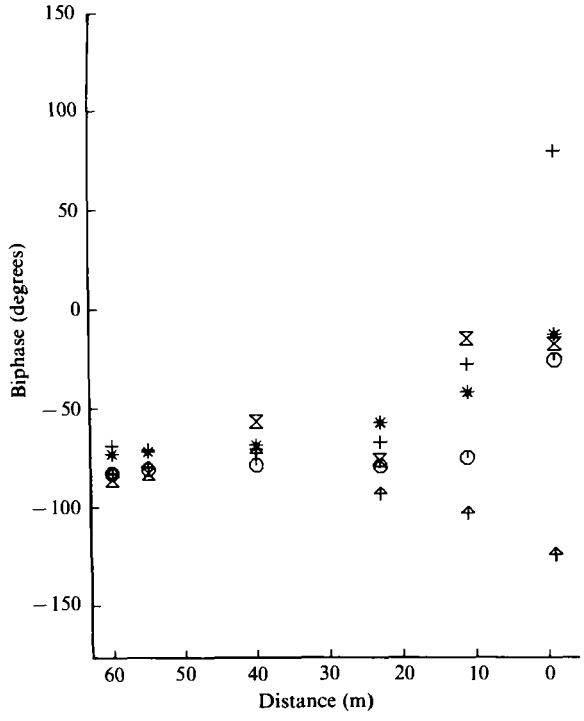

FIGURE 11. Biphase *versus* distance for selected frequency pairs as predicted by the flat-bottom spectral nonlinear model (S3). Symbols are defined in figure 2.

evolution toward $\beta = -\frac{1}{2}\pi$, similar to the field data (figure 2). The absolute value of asymmetry monotonically increases from a near-zero value to about 1 (figure 12), similar to the sloping-bottom cases (S0–S2, figures 3, 8, and 13). On the other hand, the skewness evolution on the sloping bottom is significant (figures 3, 8, and 13), but on the flat bottom varies only slightly from its initial value. The initial values of skewness for S3–S5 (band-pass filtered between $f = 0.04$ and 0.4 Hz) were 0.20, −0.02, and 0.37 respectively, and the corresponding values at $x = 61$ m were 0.16, −0.02, and 0.28.

There is little difference in the asymmetry evolution on flat and sloping bottoms, but substantial difference in the skewness evolution. Since the asymmetry is several times larger than the skewness, the major bispectral features are not bottom-slope dependent, at least for the range of slopes considered. This is not unexpected since previous model testing (Freilich & Guza 1984) indicated that bottom slope plays only a minor role in power-spectral evolution. The sloping bottom appears in (3.1) explicitly only as a linear term, and affects the nonlinear terms only implicitly through the dependence of the coupling coefficients on the dispersion relationship.

3.3. *Effects of initial phase coupling*

Given that weakly dispersive nonlinear equations support waves of permanent form, and that these waves have particular phase relationships between the various Fourier modes, it is also conceivable that bispectral evolution could depend on details of the phase coupling present in the initial conditions. The S1 model predictions of bispectra discussed in §3.1 used measured Fourier phases (which can have significant phase

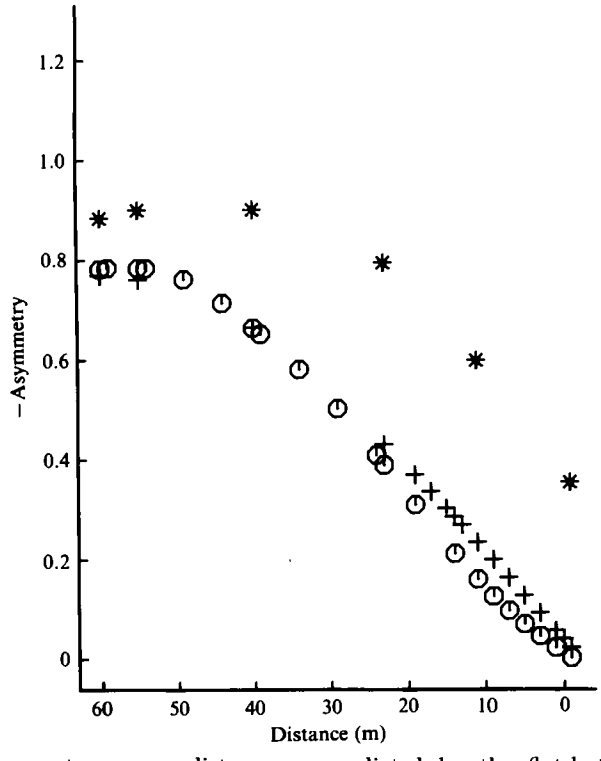

FIGURE 12. Asymmetry *versus* distance as predicted by the flat-bottom spectral nonlinear model. ⊙, S3; +, S4; ∗, S5. The data have been band-pass filtered between $f = 0.04$ and 0.4 Hz.

coupling, figures 2 and 6) as initial conditions. To see the effects of phase coupling in a typical ocean spectrum, these S1 model results (and field data) are compared with simulations with identical initial power spectra, but random initial phases (case S2, table 1). Simulations of waves propagating in a constant water depth of 2.5 m, with identical initial power spectra but different initial phase coupling, were also performed (S3 and S4). The 9 m depth measured energy spectrum (figure 9) was used as an initial condition for S3 and S4 (table 1). The harmonic content and amount of phase coupling measured in 9 m depth is less than that measured in shallower water. The differences between the initial conditions of S1 and S2, and between S3 and S4, are in the amount of phase coupling. Model sets S2 and S4 have statistically zero initial skewness and asymmetry; set S1 has more coupling than S3. As shown in figure 13, S2 evolves nearly as rapidly as S1. Sets S3 and S4 are also comparable (figure 12). It appears that the gross trends in the nonlinear evolution of asymmetry and skewness do not depend critically on the initial phase coupling, at least for the initial phases in the present data set.

The insensitivity to bottom slope and initial phase coupling is not inconsistent with the assertion (Svendsen & Buhr-Hansen 1978; Flick *et al.* 1981) that bottom slope plays a critical role in the nonlinear evolution of Stokes and cnoidal waves. Measured ocean initial conditions (many data sets have been examined) are simply not consistent with cnoidal waves. Dispersive and nonlinear terms which cancel in the special case of a cnoidal wave do not generally cancel in the ocean, and the bottom slope and special phase effects which control the cnoidal-wave evolution are small relative to the nonlinear effects which dominate in general.

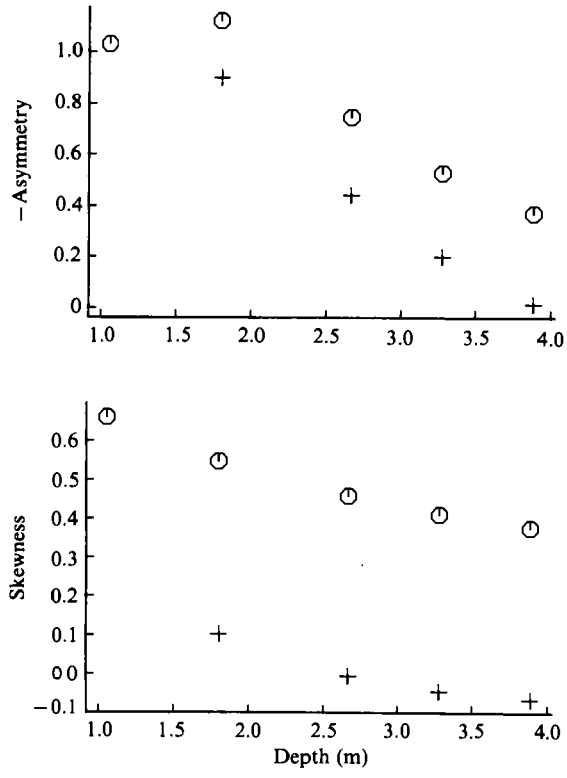

FIGURE 13. Asymmetry *versus* depth (top) and skewness *versus* depth (bottom) for the model sets S1 (⊙) and S2 (+). The data have been band-pass filtered between $f = 0.04$ and 0.4 Hz.

4. A simplified model

For the case of unidirectional waves propagating over a flat bottom, the Boussinesq equations leading to the nonlinear model (3.1) reduce to the Korteweg–de Vries equation

$$\eta_t + C\left(1+\frac{3}{2h}\eta\right)\eta_x + \gamma\eta_{xxx} = 0, \tag{4.1}$$

where $C = (gh)^{\frac{1}{2}}$, g is the acceleration due to gravity, $\gamma = \frac{1}{6}Ch^2$, and subscripts t and x denote differentiation with respect to time and space respectively. Let the sea surface be represented as

$$\eta(x,t) = \sum_n A_n(x)\exp[-\mathrm{i}(k_n x - \omega_n t)] + A_n^*(x)\exp[\mathrm{i}(k_n x - \omega_n t)], \tag{4.2}$$

where the complex Fourier amplitudes $A_n(x)$ are spatially slowly varying (rather than temporally, Bryant 1973), and the linear wavenumber

$$k_n = (\omega_n/(gh)^{\frac{1}{2}})\,(1 + (h\omega_n^2/6g) + O(\omega_n^2 h/g)^2).$$

Retaining terms of $O(A_x)$, applying the resonance condition (Bryant 1973), and

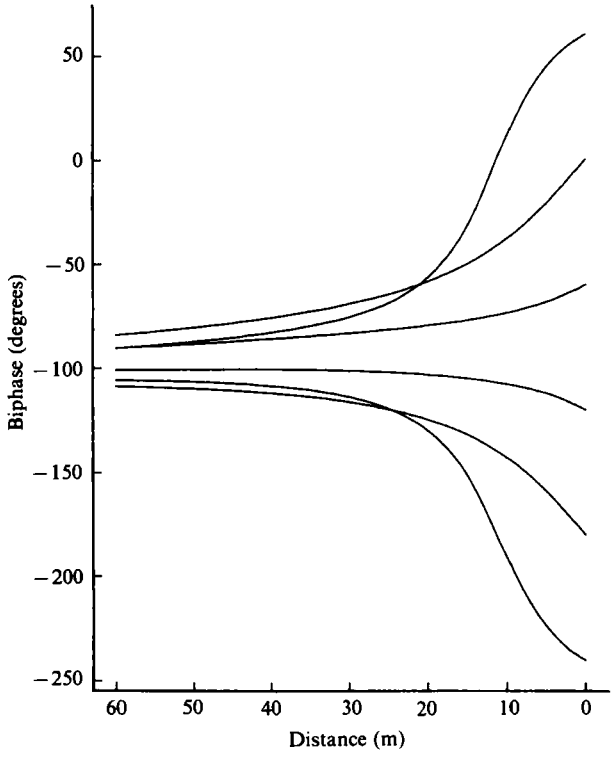

FIGURE 14. Biphase predicted by the simple harmonic-growth model ((4.6)) *versus* evolution distance. $|A_1| = 0.15$ m, $|A_2(0)| = 0.015$ m (these amplitudes correspond to a wave height of 0.66 m), $h = 2.5$ m, $f_1 = 0.067$ Hz, and at $x = 0$, $b^2 = 1$. The different lines correspond to different initial biphases.

considerable algebraic simplification leads to

$$\dot{A}_n(x) = \frac{3i}{2h} \sum_{p=1}^{\frac{1}{2}(n-1),\frac{1}{2}n} D k_p A_{n-p} A_p \exp[-i(k_{n-p}+k_p-k_n)x]$$

$$-\sum_p k_p A_{n+p} A_p^* \exp[-i(k_{n+p}-k_p-k_n)x]$$

$$+\sum_p k_p A_p A_{p-n}^* \exp[-i(k_p-k_{p-n}-k_n)x)], \tag{4.3}$$

where

$$D = \begin{cases} 1 & \text{if } p = \frac{1}{2}n, \\ \frac{1}{2} & \text{if } p \neq \frac{1}{2}n. \end{cases}$$

For the special case of a single primary wavetrain and its first harmonic there are analytic solutions to (4.3) in terms of the sine elliptic functions (Mei & Ünlüata 1972). If $A_2 \ll A_1$, then A_1 is approximately constant and

$$A_2(x) = \frac{Q}{K} A_1^2 [e^{iKx} - 1] + A_2(0), \tag{4.4}$$

where $Q = 3k_1/2h$, and the mismatch $K = k_2 - 2k_1 = \omega_1^3 (gh)^{\frac{1}{2}}/g^2$.

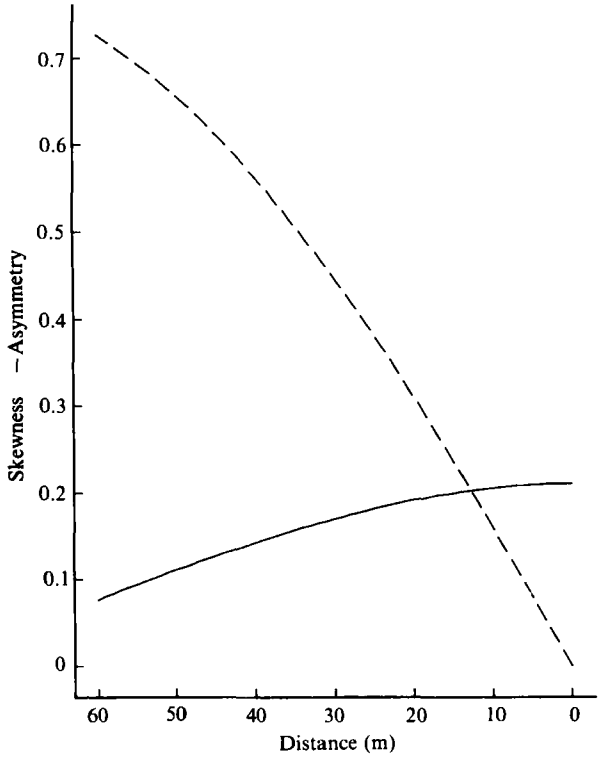

FIGURE 15. Skewness and −asymmetry predicted by the simple harmonic-growth model ((4.6)) *versus* evolution distance. The initial biphase = 0, and other parameters are the same as figure 14. Solid line, skewness; dashed line, −asymmetry.

Equation (4.4) can be rewritten in terms of the Ursell number $Ur = (A_1 k_1)/(k_1 h)^3$:

$$A_2(x) = \tfrac{3}{2} Ur A_1 [\exp[\mathrm{i}(k_1 h)^2 k_1 x] - 1] + A_2(0). \tag{4.5}$$

The Ursell number is often used as the scaling parameter for shallow water. However, as suggested by (4.5), better scaling might be obtained by modulating the Ursell number with a term related to the evolution distance and the shallowness (the exponential term in the brackets). For example, consider the limiting cases of waves arriving at a particular shallow-water location X by (*a*) travelling a long distance over a very gently sloping bottom; and by (*b*) travelling over a very steeply sloping bottom. In both cases, the Ursell number at X is approximately the same, but clearly case (*a*) has undergone more nonlinear evolution than case (*b*). This dependence on evolution distance and shallowness is consistent with the flat-bottom simulations of §3.2, where the evolution distances required to reach equivalent states reflected the depth.

The bispectrum of the self–self wave interaction described by (4.4) is, taking statistical averages (Kim *et al.* 1980),

$$B(\omega_1, \omega_1) = \frac{Q}{K} |A_1|^4 [\mathrm{e}^{-\mathrm{i}Kx} - 1] + B_0, \tag{4.6}$$

where the initial amount of phase coupling (i.e. bicoherence) between the primary and its harmonic is simulated by

$$B_0 = [A_1 A_1 A_2^*(0)] b^2,$$

where $0 \leqslant b^2 \leqslant 1$. The evolution (4.6) of bispectral quantities for parameters roughly corresponding to the field data of figures 1–3 is displayed in figures 14 and 15. Figure 14 shows a convergence toward a final biphase value of $\beta = -\frac{1}{2}\pi$, independent of the initial biphase. For small Kx ($Kx \leqslant 0.23$ for $x \leqslant 61$ m) the real part of the bispectrum (skewness) slowly decreases from its initial value, while the magnitude of the imaginary part (asymmetry) increases linearly ((4.6) and figure 15). This bispectral behaviour is qualitatively consistent with both the field observations and the model results with 205 Fourier modes (compare figure 14 with figures 2, 6, and 11, and figure 15 with figures 3, 8, 12, and 13). It seems that the simplified model embodies much of the physics that lead to the steepening of forward faces, which is a precursor of wave breaking. Note that the simplified model ((4.4)–(4.6)) is periodic. The numerical results with 205 modes are also suggestive of periodic (recurrence) behaviour for long evolution distances. In the many-mode case this periodicity appears to be largely an artifact associated with the imposition of a high-frequency cutoff which prevents the transfer of energy to even higher frequencies. Thus, the relevance of the simplified-model results is probably restricted to small Kx, and only small-Kx results are presented here. These results do not imply that recurrence phenomena play an important role in the shoaling of naturally occurring waves.

5. Conclusions

A nonlinear model (Freilich & Guza 1984) based on the Boussinesq equations for waves on a shallow, sloping bottom (Peregrine 1967) accurately predicts the observed bispectral evolution of waves shoaling on a beach (§3.1). Model predictions of bicoherence, biphase, and sea-surface-elevation skewness and asymmetry match the field observations quite well for several different data sets. Numerical simulations of waves propagating over a shallow flat bottom (§3.2) duplicate many features of the bispectral evolution observed in field data with a gently sloping bottom, suggesting that important aspects of the evolution of the bispectrum of shoaling surface gravity waves are primarily due to the nonlinear dynamics of the wave field.

Numerical integration of the model with identical energy spectra, but differing amounts of nonlinear phase coupling in the initial conditions (§3.3), indicates that the patterns of nonlinear evolution (e.g. bicoherence, biphase and asymmetry) of typical ocean wave fields are insensitive to the initial phase coupling. With the important exception of skewness, it appears that the gross statistical features of nonlinear evolution can be modelled without accurate specification of the nonlinear effects in intermediate and deep water which determine the details of the phase coupling in shallow-water initial conditions. Indeed, the evolution of bicoherence, biphase, and asymmetry for all five model sets (table 1) and the field data are remarkably similar to each other, and to many other ocean observations.

M. H. Freilich helped adapt his numerical integration code for the flat-bottom simulations. Support was provided by a grant from the Foundation for Ocean Research (Steve Elgar) and by the Office of Naval Research, Coastal Sciences Branch, under contract number N0014-75-C-0300 (R. T. Guza). The data collection was supported by ONR and the Sea Grant Nearshore Sediment Transport Study (project number RICA-N-40).

REFERENCES

BRYANT, P. J. 1973 Periodic waves in shallow water. *J. Fluid Mech.* **59**, 625–644.

ELGAR, S. & GUZA, R. T. 1985*a* Shoaling gravity waves: comparisons between field observations, linear theory, and a nonlinear model. *J. Fluid Mech.* **158**, 47–70.

ELGAR, S. & GUZA, R. T. 1985*b* Observations of bispectra of shoaling surface gravity waves. *J. Fluid Mech.* **161**, 425–448.

FLICK, R. E., GUZA, R. T. & INMAN, D. L. 1981 Elevation and velocity measurements of laboratory shoaling waves. *J. Geophys. Res.* **86**, 4149–4160.

FREILICH, M. H. & GUZA, R. T. 1984 Nonlinear effects on shoaling surface gravity waves. *Phil. Trans. R. Soc. Lond.* A **31**, 1–41.

HASSELMAN, K., MUNK, W. & MACDONALD, G. 1963 Bispectra of ocean waves. In *Time Series Analysis* (ed. M. Rosenblatt), pp. 125–139. Wiley.

HAUBRICH, R. A. 1965 Earth noises, 5 to 500 millicycles per second, 1. *J. Geophys. Res.* **70**, 1415–1427.

KIM, Y. C. & POWERS, E. J. 1979 Digital bispectral analysis and its application to nonlinear wave interactions. *IEEE Trans. on Plasma Science*, **1**, 120–131.

KIM, Y. C., BEALL, J. M., POWERS, E. J. & MIKSAD, R. W. 1980 Bispectrum and nonlinear wave coupling. *Phys. Fluids* **23**, 250–263.

MEI, C. C. & ÜNLÜATA, U. 1972 Harmonic generation in shallow water waves. In *Waves on Beaches and Resulting Sediment Transport* (ed. R. Meyer), pp. 181–202. Academic.

PEREGRINE, D. H. 1967 Long waves on a beach. *J. Fluid Mech.* **27**, 815–827.

SVENDSEN, I. A. & BUHR-HANSEN, J. 1978 On the deformation of periodic long waves over a gently sloping bottom. *J. Fluid Mech.* **87**, 433–448.